

Aerial Assistive Payload Transportation Using Quadrotor UAVs with Nonsingular Fast Terminal SMC for Human Physical Interaction

Hussein Naser, Hashim A. Hashim, and Mojtaba Ahmadi

Abstract—This paper presents a novel approach to utilizing underactuated quadrotor Unmanned Aerial Vehicles (UAVs) as assistive devices in cooperative payload transportation task through human guidance and physical interaction. The proposed system consists of two underactuated UAVs rigidly connected to the transported payload. This task involves the collaboration between human and UAVs to transport and manipulate a payload. The goal is to reduce the workload of the human and enable seamless interaction between the human operator and the aerial vehicle. An Admittance-Nonsingular Fast Terminal Sliding Mode Control (NFTSMC) is employed to control and asymptotically stabilize the system while performing the task, where forces are applied to the payload by the human operator dictate the aerial vehicle's motion. The stability of the proposed controller is confirmed using Lyapunov analysis. Extensive simulation studies were conducted using MATLAB, Robot Operating System (ROS), and Gazebo to validate robustness and effectiveness of the proposed controller in assisting with payload transportation tasks. Results demonstrates feasibility and potential benefits utilizing quadrotor UAVs as assistive devices for payload transportation through intuitive human-guided control.

Index Terms—Cooperative payload transportation, Admittance control, Sliding mode control, Quadrotor control

I. INTRODUCTION

A. Motivation

B. Background

ASSISTIVE technology has gained significant interest in the field of robotics in recent years. It plays a crucial role in various domains, including rehabilitation [1]–[5], aerial manipulation systems [6], [7], logistics [8], [9], precision agriculture [10], [11], and construction [12]–[14] by enhancing human capabilities and facilitating complex tasks. Underactuated quadrotor UAVs with their low cost, simple mechanical design, maneuverability, and, versatility offer promising potential as assistive devices in many fields. They can be used for assistive payload transportation through human physical interaction. This involves collaboration between human and quadrotors to transport and manipulate a payload. The goal of such collaborative systems is to reduce the workload of human and enable intuitive interaction between the operator and the aerial transportation system. Single quadrotors have been used in payload transportation to help human in delivering packages and medical supplies [15]–[17]. Although

using a single quadrotor in delivery operations has proven its effectiveness, it suffers from low weight capacity of the transported payload [18]–[20]. To overcome such problem, researchers have explored cooperative payload transportation in different configurations such as dual or multiple agents with suspended-load transportation. Different techniques and control algorithms have been proposed to achieve the cooperative transportation task [18], [21]–[29].

C. Related Work

Design of a control algorithm for moving vehicles has been deemed a challenging task [18], [20], [30]–[35]. Tagliabue et al. [34] introduced a collaborative object transportation system using Micro Aerial Vehicles (MAVs) by employing a passive force control approach. They adopted a master-slave framework, employing an admittance controller to ensure the slave unit's compliance with external forces exerted by the master MAV on the payload. To estimate the external force on the slave, they utilized an Unscented Kalman Filter depending on data from a Visual-Inertial navigation system. The system was implemented for outdoor applications to transport a 1.2-meter-long object. Horyna et al. [35] introduced a control approach for a system of two UAVs carrying a beam-type payload for outdoor applications. A master-slave control architecture comprises a feedback controller and a Model Predictive Control (MPC) reference tracker was implemented on the master agent's side, with the slave agent acting as an actuator following the master's directives. Loianno and Kumar [36] developed a collaborative transportation aerial system using a team of small quadrotors. They introduced a method for coordinated control that allows for independent control of each quadrotor while maintaining the stability of the system. The authors suggested a cooperative localization strategy that uses the information on the inherent rigidity of the structure to deduce additional constraints between the poses of the vehicles. This formulation casts the pose estimation challenge as an optimization problem on the Lie group of the Special Euclidean Group $SE(3)$ [37] and the Lie group of the Special Orthogonal Group $SO(3)$ [38]. Rajaeizadeh et al. [39] explored the challenge of coordinating pair of quadrotors rigidly connected to the payload for cooperative transportation. They introduced a rigid-body formation control system utilizing the Linear Quadratic Regulator (LQR) method, along with a Paparazzi-based guidance approach for generating the trajectory of transportation mission. The system

This work was supported in part by the National Sciences and Engineering Research Council of Canada (NSERC), under the grants RGPIN-2022-04937.

H. Naser, H. A. Hashim, and M. Ahmadi are with the Department of Mechanical and Aerospace Engineering, Carleton University, Ottawa, Ontario, K1S-5B6, Canada (e-mail: hhashim@carleton.ca).

results were validated through simulations. Mellinger et al. [40] examined the challenge of controlling multiple quadrotors to collaboratively grasp and transport a payload. The system was modeled using a rigid connection between multiple UAVs and the payload. The authors conducted an experimental investigation involving teams of quadrotors working together to grasp, stabilize, and transport payloads along predefined three-dimensional paths.

The aforementioned methods of payload transportation depends on preprogrammed trajectories or remote control, limiting their capabilities in dynamic environments through physical interaction. Recent advances in control strategies have paved the way for intuitive human-robot interactions, allowing seamless collaboration between human operators and autonomous systems. By integrating admittance control with quadrotors, it becomes possible to harness the intuitive physical interaction capabilities of human to guide the motion of the aerial vehicles during payload transportation tasks. Augugliaro and D'Andrea [41] examined the implementation of admittance control on a single quadrotor for the physical interaction between a human and an aerial vehicle. Admittance control enables developers to modify the virtual inertia, damping, and stiffness of the aerial vehicle facilitating physical interaction. External forces acting on the quadrotor are measured using sensors or inferred from position and orientation data and fed into the admittance controller which adjusts the vehicle's intended path accordingly. This trajectory is then followed by the inner position and orientation controllers.

Prajapati and Vashista [42] investigated the possible uses of physical interaction between human and aerial vehicles in outdoor environments. They introduced a setup involving a rigid object lifted by both a human and a quadcopter from its extremities. A custom sensor systems designed to interpret human commands and provide reliable state feedback. Linearization of the dynamic equations of the system and state-feedback control techniques were utilized to control the quadrotor for collaborative payload transportation. Xu et al. [43] introduced a visual impedance control approach for collaborative transportation between a human and a tethered aerial vehicle. Using the force of the cable and the features of the visual objects as feedback, the aerial vehicle follows the human operator. The proposed technique incorporates a vision-based velocity observer to estimate the relative velocity between the aerial vehicle and the human. The system is designed for indoor application where a human participant transported a bar with the assistance of the tethered aerial vehicle. In Romano et al. [44], a cooperative payload transport system guided by haptic feedback was investigated. This system comprises a team of five quadrotors linked to a payload via tethers. The Human partner can provide haptic guidance commands by exerting force on the suspended payload, and the system estimates the applied force and its direction. A centralized payload controller directs the quadrotors to follow the desired trajectory.

There are several limitations and shortcomings can be identified in the existing methods of the payload transportation. In one hand, these methods involve preprogrammed tasks and/or remote-control requirements which restricts their adaptability

and usability in unstructured work environments. On the other hand, other methods use cables and tethers in physical interaction configurations, which pose challenges and difficulties, especially when dealing with aerial vehicles. Cables can get entangled during missions, causing instability, potential system damage, and low safety for human partners. Additionally, cable-suspended payloads suffer from oscillation which introduces complexity to the system's dynamics and requires complex control algorithms to stabilize the transportation system. The oscillation also introduces difficulty to implement the admittance controller for physical interaction, as it is hard to distinguish between the oscillation and the input of the interaction forces. Furthermore, this issue significantly affects battery energy consumption, limiting the mission duration.

D. Motivation and Contribution

To tackle these challenges, we implemented rigid connections between the underactuated quadrotor UAVs and the transported payload. This configuration offers distinct advantages, providing unified dynamics of the quadrotors and the payload, improving operator safety, and enabling precise measurement of physical interactions. In this paper, we propose a novel assistive aerial system in which two quadrotors are employed for payload transportation following human guidance through physical interaction. The aerial vehicle lifts the payload to a comfortable operating altitude, allowing the human operator to interact and guide the system by applying force directly to the payload without carrying it. An admittance controller is utilized to translate the forces applied to the payload by the human operator into motion commands for the quadrotors, ensuring intuitive and responsive control. The admittance control algorithm considers the system as a mass-damper-spring system, where the quadrotors act as dampers and the payload as a mass connected to a spring. When a force is applied to the payload, the system responds by moving in the direction of the applied force, simulating the behavior of a mass-spring-damper system. This approach enables the aerial vehicle to adaptively adjust its motion based on the forces exerted by the human operator, providing a natural and intuitive control interface. The paper contributions are summarized as follows:

- Design of an assistive cooperative payload transportation system with human physical interaction.
- A model of rigidly connected mechanical system is derived for the sake of analysis and control.
- Design and implementation of an admittance controller to enable aerial vehicle-human physical interaction.
- Nonsingular Fast Terminal Sliding Mode Control (NFTSMC) is proposed to control and asymptotically stabilize the system to track human guidance and achieve the transportation task. Lyapunov stability approach has been utilized to ensure system stability.

E. Paper Structure

The rest of the paper is organized as follows: Section II presents a comprehensive overview of the tools, methods, preliminaries, and problem formulation. Section III provides a detailed explanation of the controller design and stability

analysis. Simulation setup and implementation and numerical results are elaborated upon in Section IV. Finally, Section V concludes the article and outlines avenues for future work.

II. PRELIMINARIES AND PROBLEM FORMULATION

In this work, our objective is to design and implement an assistive aerial system to assist humans in payload transportation with human physical interaction and guidance. The proposed system consists of two quadrotors collaboratively lifting and transporting a common payload that is rigidly connected to the quadrotors. The human operator can interact with the assistive aerial system through force feedback, allowing intuitive control of the system during payload transportation tasks. The human operator can directly push or apply forces to the transported payload to guide the system in any direction in three-dimensional (3D) space. The applied force can be measured using either a one force-torque sensor attached to the center of mass (CoM) of the payload or two force-torque sensors attached at the points of the rigid connection of each quadrotor with the payload ends. The dynamic model of each component of the assistive system (two quadrotors and the payload) will be given separately; then the dynamic model for the entire system will be derived in detail for control purposes. Without loss of generality, the entire system will be considered as one rigid body and treated as one aerial vehicle. All the notations, parameters, and symbols used in this paper are illustrated in the following tables. For notations and symbols related to the modeling of individual quadrotor, payload, entire assistive system, controller-related notations and symbols respectively, refer to Table I.

A. System Model

For the modeling purposes, we assign a global world inertial reference frame $\mathcal{I}_G = \{O, X, Y, Z\}$ and a body-fixed reference frame $L_F = \{o, x_L, y_L, z_L\}$ attached to the CoM of the payload as well as a reference frame $\mathcal{B}_i = \{o_i, x_{B_i}, y_{B_i}, z_{B_i}\}$ attached to the CoM of each quadrotor where $i = 1 \dots N$ ($N = 2$ for the system in this work). All reference frames have a positive z axis pointing upward (gravity is negative). Let $p_i = [x_i, y_i, z_i]^T$ and $v_i = \dot{p}$ be the translational position and velocity of the quadrotor, respectively, defined in \mathcal{I}_G , $\omega = [p, q, r]^T$ be the vector of angular rates defined in the body-fixed frame, and $\Theta = [\phi, \theta, \psi]^T$ be the vector of Euler angles, roll, pitch, and yaw that represent the attitude of the aerial vehicle in \mathcal{I}_G . $R \in SO(3)$ represents the rotation matrix from the body-fixed frame to \mathcal{I}_G described with respect to the Special Orthogonal Group $SO(3)$ where R has a determinant of $+1$ and $RR^T = \mathbf{I}_3$ with \mathbf{I}_3 being an identity matrix with dimension 3-by-3 [38], [45], [46]. The rotation matrix R follows the convention of $Z - X - Y$ of Euler angles and is given by [45]:

$$\mathbf{R} = \begin{bmatrix} c\theta c\psi - s\phi s\theta s\psi & -c\phi s\psi & s\theta c\psi + s\phi c\theta s\psi \\ c\theta s\psi + s\phi s\theta c\psi & c\phi c\psi & s\theta s\psi - s\phi c\theta c\psi \\ -c\phi s\theta & s\phi & c\phi c\theta \end{bmatrix} \quad (1)$$

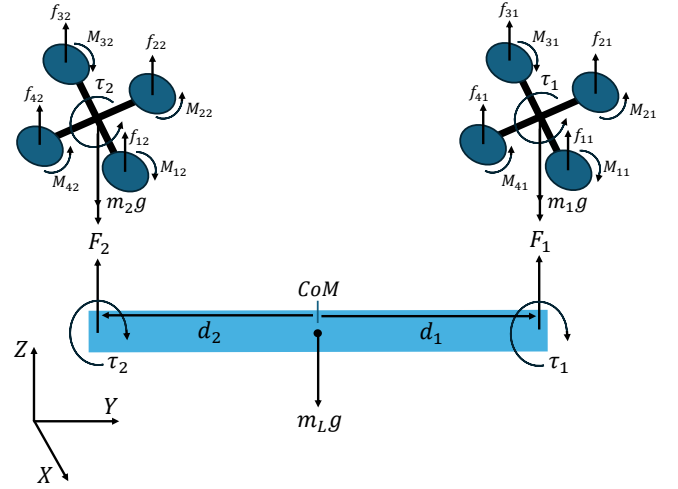


Fig. 1: Free body diagram of the entire system components.

where $c\phi$ and $s\phi$ denote $\cos(\phi)$ and $\sin(\phi)$, respectively. The relationship between ω and the rate of change of the Euler angles $\dot{\Theta} = [\dot{\phi}, \dot{\theta}, \dot{\psi}]^T$ is described by [45]:

$$\begin{bmatrix} p \\ q \\ r \end{bmatrix} = \begin{bmatrix} c\theta & 0 & -c\phi s\theta \\ 0 & 1 & s\phi \\ s\theta & 0 & c\phi c\theta \end{bmatrix} \begin{bmatrix} \dot{\phi} \\ \dot{\theta} \\ \dot{\psi} \end{bmatrix} \quad (2)$$

1) *Individual Quadrotor Dynamics*: Using the Newton-Euler method and referring to Figure 1, the translational and rotational dynamic model of the individual underactuated quadrotor UAV is given as follows [18], [20]:

$$\begin{aligned} m_i \dot{v}_i &= R \begin{bmatrix} 0 \\ 0 \\ u_{1_i} \end{bmatrix} - \begin{bmatrix} 0 \\ 0 \\ m_i g \end{bmatrix} - F_i \\ J_i \dot{\omega} &= \begin{bmatrix} u_{2_i} \\ u_{3_i} \\ u_{4_i} \end{bmatrix} - \begin{bmatrix} p \\ q \\ r \end{bmatrix} \times J_i \begin{bmatrix} p \\ q \\ r \end{bmatrix} - \tau_i \end{aligned} \quad (3)$$

where $m_i \in \mathbb{R}$ is the mass, $J_i \in \mathbb{R}^{3 \times 3}$ is the moment of inertia, $\dot{v}_i \in \mathbb{R}^3$ is the translational acceleration, $u_{1_i} \in \mathbb{R}$ is the total thrust measured in the body-fixed reference frame, and $[u_{2_i}, u_{3_i}, u_{4_i}]^T$ are the rolling, pitching, and yawing moments in $x_{B_i}, y_{B_i}, z_{B_i}$ axes of each individual quadrotor, respectively, $g \in \mathbb{R}$ is the gravity, $\dot{\omega} \in \mathbb{R}^3$ is the angular acceleration which is the same for all components of the system due to rigid connection, and $F_i \in \mathbb{R}^3$ and $\tau_i \in \mathbb{R}^3$ are the force and torque of the rigid interconnection between the two quadrotors and the payload, respectively.

The total thrust and moments of individual quadrotor are given as follows:

$$\begin{aligned} u_{1_i} &= \sum_{j=1}^4 f_{j_i} \\ \begin{bmatrix} u_{2_i} \\ u_{3_i} \\ u_{4_i} \end{bmatrix} &= \begin{bmatrix} l(f_{2_i} - f_{4_i}) \\ l(f_{3_i} - f_{1_i}) \\ M_{1_i} - M_{2_i} + M_{3_i} - M_{4_i} \end{bmatrix} \end{aligned} \quad (4)$$

where $(f_{j_i} = k_t \Omega_{j_i}^2)$ is the thrust generated by each rotor of individual quadrotor, and it is proportional to the square of the

TABLE I: Nomenclature.

System related parameters		
Symbol	Definition	Unit
$\mathcal{I}_G / \mathcal{B}_i$	Inertial-frame / i UAV body frame.	-
L_F	Payload body-fixed-frame.	-
N	Number of UAVs.	-
$g \in \mathbb{R}$	Gravitational acceleration.	$[m/s^2]$
$p_i \in \mathbb{R}^3$	i UAV position in \mathcal{I}_G .	$[m]$
$v_i \in \mathbb{R}^3$	i UAV linear velocity in \mathcal{I}_G .	$[m/s]$
$\dot{v}_i \in \mathbb{R}^3$	i UAV linear acceleration in \mathcal{I}_G .	$[m/s^2]$
$m_i \in \mathbb{R}$	i UAV mass.	$[kg]$
$J_i \in \mathbb{R}^{3 \times 3}$	i UAV moment of inertia.	$[kg \ m^2]$
$\Omega_{ji} \in \mathbb{R}$	Angular speed of j rotor of i quadrotor.	$[rpm]$
$k_t \in \mathbb{R}$	Thrust (lift) constant.	$[N/rpm^2]$
$k_m \in \mathbb{R}$	Moment (drag) constant.	$[N.m/rpm^2]$
$l \in \mathbb{R}$	Distance from CoM.	$[m]$
p_L, v_L, \dot{v}_L	Payload position, linear velocity, linear acce. in \mathcal{I}_G .	
m_L, J_L	Payload mass and moment of inertia.	
$F_i \in \mathbb{R}^3$	i UAV force exerted on payload.	$[N]$
$\tau_i \in \mathbb{R}^3$	i UAV torque exerted on payload.	$[N.m]$
p_s, v_s, \dot{v}_s	System position, linear velocity, and acce. in \mathcal{I}_G .	
$R \in SO(3)$	Rotation matrix in body-frame.	-
$\omega, \dot{\omega}$	Angular velocity and acce. of the system in \mathcal{B}_i .	-
(ϕ, θ, ψ)	Roll, pitch, and yaw Euler angles.	$[rad]$
m_t, J_t	Total mass and moment of inertia of entire system.	-
$F_t \in \mathbb{R}$	Total thrust produced by two quadrotors.	$[N]$
$U_t \in \mathbb{R}^3$	Total (rolling, pitching, yawing) moments.	$[N.m]$
$F_{drag} \in \mathbb{R}^3$	Aerodynamic drag force acting on the system.	$[N]$
$M_{drag} \in \mathbb{R}^3$	Aerodynamic drag moment acting on the system.	$[N.m]$
$D_l \in \mathbb{R}^3$	Translational external disturbances.	$[N]$
$D_r \in \mathbb{R}^3$	Rotational external disturbances.	$[N.m]$
Controller Related Parameters and Symbols		
Symbol	Definition	Unit
$\chi \in \mathbb{R}^3$	Actual position and orientation of the entire system	-
$\chi_d \in \mathbb{R}^3$	Desired position and orientation of the entire system	-
$e \in \mathbb{R}^6$	Tracking error	-
$S \in \mathbb{R}^6$	Sliding surface	-
$\xi \in \mathbb{R}^{6 \times 6}$	Positive diagonal matrix of control constants	-
$\eta \in \mathbb{R}^{6 \times 6}$	Positive diagonal matrix of control constants	-
$a \in \mathbb{R}$	Positive constant	-
$\lambda_1 \in \mathbb{R}^{6 \times 6}$	Positive diagonal matrix of control constants	-
$\lambda_2 \in \mathbb{R}^{6 \times 6}$	Positive diagonal matrix of control constants	-
$V > 0$	Positive definite Lyapunov function for the system	-
(u_x, u_y, u_z)	Virtual control inputs	-
$U_1 \in \mathbb{R}$	Designed total thrust control input	$[N]$
$U_2 \in \mathbb{R}$	Designed total rolling moment of entire system	$[N.m]$
$U_3 \in \mathbb{R}$	Designed total pitching moment of entire system	$[N.m]$
$U_4 \in \mathbb{R}$	Designed total yawing moment of entire system	$[N.m]$
$M \in \mathbb{R}^{3 \times 3}$	Virtual mass for admittance controller	$[kg]$
$C \in \mathbb{R}^{3 \times 3}$	Virtual damping coefficients for admittance controller	$[N.s/m]$
$K \in \mathbb{R}^{3 \times 3}$	Virtual spring constants for admittance controller	$[N.s/m]$
$T_d \in \mathbb{R}^3$	Desired trajectory of admittance controller	$[m]$
$T_r \in \mathbb{R}^3$	Reference trajectory generated by admittance controller	$[m]$

angular speed (Ω_{ji}) of the rotor, k_t is the thrust (lift) constant, ($M_{ji} = k_m \Omega_{ji}^2$) is the moment produced by each rotor, k_m is the moment (drag) constant, and l is the distance from the CoM of the quadrotor to the axis of rotation of the rotors. The total thrust and moments in Equation (4) can be combined to form the input vector for each individual quadrotor as given in Equation (5) [18], [24]:

$$\begin{bmatrix} u_{1i} \\ u_{2i} \\ u_{3i} \\ u_{4i} \end{bmatrix} \begin{bmatrix} 1 & 1 & 1 & 1 \\ 0 & l & 0 & -l \\ -l & 0 & l & 0 \\ \mu & -\mu & \mu & -\mu \end{bmatrix} \begin{bmatrix} f_{1i} \\ f_{2i} \\ f_{3i} \\ f_{4i} \end{bmatrix} \quad (5)$$

where ($\mu = k_m/k_t$) is the relationship between the thrust and moment constants.

2) *Payload Dynamics*: Let $p_L = [x_L, y_L, z_L]^T$ and $v_L = \dot{p}_L$ be the translational position and velocity of the CoM of the payload, respectively, defined in the inertial reference frame. Referring to Figure 1, the translational and rotational dynamics of the payload are given as follows:

$$\begin{aligned} m_L \dot{v}_L &= (F_1 + F_2) - \begin{bmatrix} 0 \\ 0 \\ m_L g \end{bmatrix} \\ J_L \dot{\omega} &= (\tau_1 + \tau_2) - \begin{bmatrix} p \\ q \\ r \end{bmatrix} \times J_L \begin{bmatrix} p \\ q \\ r \end{bmatrix} + (d_1 \times F_1) + (d_2 \times F_2) \end{aligned} \quad (6)$$

where $m_L \in \mathbb{R}$ is the mass, $J_L \in \mathbb{R}^{3 \times 3}$ is the diagonal matrix of the moment of inertia, $\dot{v}_L \in \mathbb{R}^3$ is the translational

acceleration, and $(F_1$ and $F_2) \in \mathbb{R}^3$ and $(\tau_1$ and $\tau_2) \in \mathbb{R}^3$ are the forces and torques exerted by the two quadrotors on the payload at the points of contact of the rigid connection. The expressions $(d_1 \times F_1)$ and $(d_2 \times F_2)$ express the moments due to the forces $(F_1$ and $F_2)$ at the points of contact and d_1 and d_2 are the vectors from the CoM of the payload to the CoM of quadrotor1 and quadrotor2, respectively, where $(d_i = p_i - p_L)$.

3) *System Kinematics*: The kinematic relationships between the payload and the two quadrotors are given in Equation (7):

$$\begin{cases} p_i &= p_L + R d_i, \\ \dot{p}_i &= \dot{p}_L + \omega \times d_i, \\ \ddot{p}_i &= \ddot{p}_L + \dot{\omega} \times d_i + \omega(\omega \times d_i), \end{cases} \quad (7)$$

4) *Dynamics of the entire system*: To formulate the dynamic equations of the entire system, let Assumption 1 hold true:

Assumption 1. *In this work, we assume the following.*

- The system is composed of three separate rigid components that are rigidly connected with their own specific physical characteristics.
- The two quadrotors are identical with the same known geometrical and physical specifications.
- The payload is a circular section beam with a mass of m_L , a length of L , and a cross-sectional radius r_L .
- The entire system is symmetric in X and Y axes.

Let $p_s = [x, y, z]^T$ and $v_s = \dot{p}_s$ be the translational position and velocity of the CoM of the entire aerial vehicle, respectively, defined in the inertial reference frame. Based on Assumption 1 and referring to Figure 1, combining the dynamics of the quadrotor in Equation (3) with the dynamics of the payload in Equation (6) as well as adding the aerodynamic drag effects and external disturbances results in formulation of the dynamics of the entire system as follows:

$$\begin{aligned} m_t \dot{v}_s &= R \begin{bmatrix} 0 \\ 0 \\ F_t \end{bmatrix} - \begin{bmatrix} 0 \\ 0 \\ m_t g \end{bmatrix} - F_{drag} + D_l \\ J_t \dot{\omega} &= U_t - \begin{bmatrix} p \\ q \\ r \end{bmatrix} \times J_t \begin{bmatrix} p \\ q \\ r \end{bmatrix} - M_{drag} + D_r \end{aligned} \quad (8)$$

where $m_t \in \mathbb{R}$ is the total mass of the entire system, and it can be given as $(m_t = m_1 + m_2 + m_L)$, $\dot{v}_s \in \mathbb{R}^3$ is the translational acceleration of the entire system, $J_t \in \mathbb{R}^{3 \times 3}$ is the total moment of inertia of the entire system, $D_l \in \mathbb{R}^3$ and $D_r \in \mathbb{R}^3$ are translational and rotational external disturbances, $(F_{drag} = K_{l_{drag}} v) \in \mathbb{R}^3$ and $(M_{drag} = K_{r_{drag}} \omega) \in \mathbb{R}^3$ are the aerodynamic drag forces and torques, $K_{l_{drag}}$ and $K_{r_{drag}}$ are positive diagonal matrices that represent the translational and rotational drag coefficients of the system, respectively, $F_t \in \mathbb{R}$ and $U_t \in \mathbb{R}^3$ are the total thrust and moments produced by the two quadrotors measured in the body-fixed frame of the system. Considering each quadrotor produces thrust and moments in its own coordinate frame, a relationship between the behavior of the entire system and the quadrotors

needs to be developed depending on the system's configuration as follows:

$$\begin{bmatrix} F_t \\ U_t \end{bmatrix} = \mathbf{B} u_q \quad (9)$$

where $\mathbf{B} \in \mathbb{R}^{4 \times 4N}$ is a constant matrix and determined based on the system configuration and the yaw angle (ψ_i) of each quadrotor with respect to the payload which is designed to be zero $(\psi_i = 0)$ for the rigid connection of the system. \mathbf{B} is given as follows:

$$\mathbf{B} = \sum_{i=1}^2 \begin{bmatrix} 1 & 0 & 0 & 0 \\ d_i(2) & 1 & 0 & 0 \\ -d_i(1) & 0 & 1 & 0 \\ 0 & 0 & 0 & 1 \end{bmatrix} \quad (10)$$

and $u_q \in \mathbb{R}^{4N}$ is the vector of the control input of the two quadrotors as given below:

$$u_q = [u_{11}, u_{21}, u_{31}, u_{41}, u_{12}, u_{22}, u_{32}, u_{42}]^T \quad (11)$$

Remark 1. *In our control scheme, the $[F_t, U_t]^T$ is firstly calculated then used to find (u_q) in (11) for the quadrotors to follow the desired tracking control. It can be clearly noticed that the system in Equation (9) is underdetermined, where there are only four equations for eight unknowns. Therefore, we need to optimize the solutions through minimizing a cost function $\mathcal{L}(u_q) : \mathbb{R}^8 \rightarrow \mathbb{R}$ such that:*

$$u_q^* = \operatorname{argmin}\{\mathcal{L}([F_t, U_t]^T = \mathbf{B} u_q)\} \quad (12)$$

where the cost function \mathcal{L} in (12) is given as follows:

$$\mathcal{L} = \sum_{i=1}^2 c_{1i} u_{1i} + c_{2i} u_{2i} + c_{3i} u_{3i} + c_{4i} u_{4i} \quad (13)$$

where c_{ji} are the cost function's coefficients that can be used to define a matrix $\mathcal{H} \in \mathbb{R}^{8 \times 8}$ such that the cost function \mathcal{L} in (13) can be redefined as $(\mathcal{L} = \|\mathcal{H} u_q\|_2^2)$, and \mathcal{H} is given as follows:

$$\mathcal{H} = \sqrt{\operatorname{diag}(c_{11}, c_{21}, c_{31}, c_{41}, c_{12}, c_{22}, c_{32}, c_{42})} \quad (14)$$

Using \mathbf{B} in (10) and \mathcal{H} in (14), the solution can be determined using pseudo inverse (Moore-Penrose inverse) as [40]:

$$\begin{aligned} u_q^* &= \mathcal{H}^{-1} (\mathbf{B} \mathcal{H}^{-1})^+ [F_t, U_t]^T \\ &= \mathcal{H}^{-2} \mathbf{B}^T (\mathbf{B} \mathcal{H}^{-2} \mathbf{B}^T)^{-1} [F_t, U_t]^T \end{aligned} \quad (15)$$

where $+$ denotes the pseudo inverse and u_q^* in (15) satisfies Remark 1.

III. CONTROLLER DESIGN AND STABILITY ANALYSIS

In this section, the controller will be designed to control the assistive payload transportation system with human physical interaction to track human guidance and stabilize the system while transporting the payload in the presence of aerodynamic drag forces and external disturbances. Figure 2 depicts a schematic diagram of the overall control system. The controller will be designed based on a novel combination of the admittance controller for human-aerial vehicle physical interaction and NFTSMC, which is a well-known nonlinear

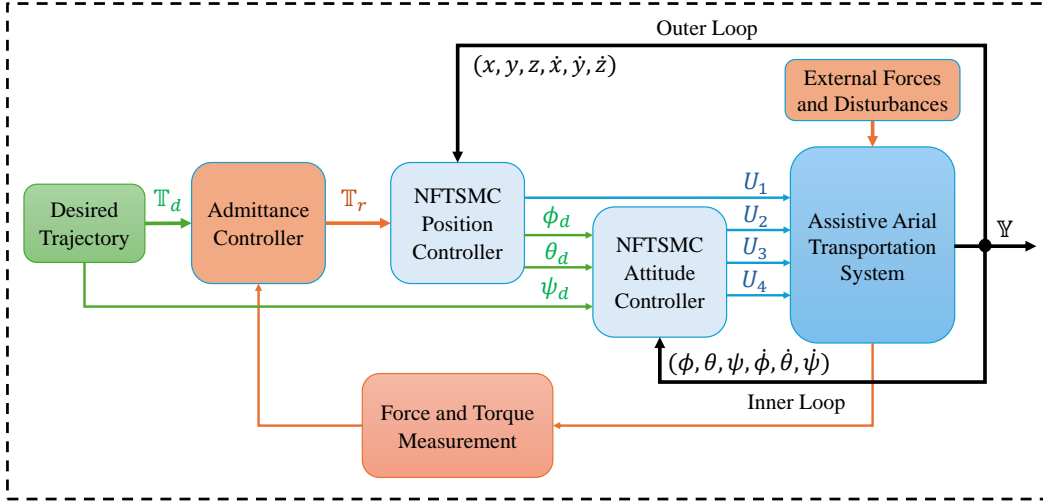


Fig. 2: Schematic block diagram of the control system.

controller in terms of its robustness against modeling uncertainties and external disturbances, as well as fast convergence to ensure system stability [18], [24], [32].

For control design purposes, the dynamic model in Equation (8) will be expanded and written in the following form:

$$\ddot{\chi} = F + \delta + bu \quad (16)$$

where $\ddot{\chi} = [\ddot{x}, \ddot{y}, \ddot{z}, \ddot{\phi}, \ddot{\theta}, \ddot{\psi}]^T$ is the vector of the system translational and angular accelerations, F and $b \neq 0$ are smooth non-linear functions, and δ represents the uncertainties and external forces and disturbances, and u is the control input.

Assumption 2. δ in Equation (16) is assumed to be bounded and satisfy $\|\delta\| \leq \varpi$, where $\varpi > 0$.

Assumption 3. The desired position of the entire system, $X_d = [x_d, y_d, z_d]$, is bounded, smooth, and differentiable.

Assumption 4. For small (ϕ, θ, ψ) angles applications such as the system in this work, the Euler angles rate, $\dot{\Theta} = (\dot{\phi}, \dot{\theta}, \dot{\psi})$ is assumed to be equal to the angular velocity $\omega = (p, q, r)$.

Let Assumptions 2, 3, and 4 hold true, the extended dynamic equations of the system are given as follows:

$$\begin{cases} \ddot{x} &= \frac{1}{m_t} [-k_{l_{dragx}} \dot{x} + d_{l_1} + (s\theta c\psi + s\phi c\theta s\psi)U_1] \\ \ddot{y} &= \frac{1}{m_t} [-k_{l_{drary}} \dot{y} + d_{l_2} + (s\theta s\psi - s\phi c\theta c\psi)U_1] \\ \ddot{z} &= \frac{1}{m_t} [-k_{l_{dragz}} \dot{z} + d_{l_3} - m_t g + (c\phi c\theta)U_1] \\ \ddot{\phi} &= \frac{1}{J_x} [(J_y - J_z)\dot{\theta}\dot{\psi} - k_{r_{drag\phi}} \dot{\phi} + d_{r_1} + U_2] \\ \ddot{\theta} &= \frac{1}{J_y} [(J_z - J_x)\dot{\phi}\dot{\psi} - k_{r_{drag\theta}} \dot{\theta} + d_{r_2} + U_3] \\ \ddot{\psi} &= \frac{1}{J_z} [(J_x - J_y)\dot{\phi}\dot{\theta} - k_{r_{drag\psi}} \dot{\psi} + d_{r_3} + U_4] \end{cases} \quad (17)$$

Remark 2. As it can be noticed from Equation (17) that the system is divided into two subsystems, namely, the position subsystem (first three lines in Equation (17)) is underactuated

subsystem with one control input (U_1) and three outputs (x, y, z) , and the orientation subsystem (last three lines in Equation (17)) is full actuated subsystem with three control inputs (U_2, U_3, U_4) and three outputs (ϕ, θ, ψ) . Therefore, the controller design needs to account for such challenging dynamical system.

In order to deal with the challenge of the underactuated subsystem in Equation (17) as remarked in Remark 2, let us consider the following virtual control inputs:

$$\begin{bmatrix} u_x \\ u_y \\ u_z \end{bmatrix} = \begin{bmatrix} (s\theta c\psi + s\phi c\theta s\psi)U_1 \\ (s\theta s\psi - s\phi c\theta c\psi)U_1 \\ (c\phi c\theta)U_1 \end{bmatrix} \quad (18)$$

Therefore, components of Equation (16) are given as follows:

$$\begin{aligned} F &= \begin{bmatrix} -\frac{1}{m_t} k_{l_{dragx}} \dot{x} \\ -\frac{1}{m_t} k_{l_{drary}} \dot{y} \\ -g - \frac{1}{m_t} k_{l_{dragz}} \dot{z} \\ \frac{(J_y - J_z)}{J_x} \dot{\theta}\dot{\psi} - \frac{k_{r_{drag\phi}}}{J_x} \dot{\phi} \\ \frac{(J_z - J_x)}{J_y} \dot{\phi}\dot{\psi} - \frac{k_{r_{drag\theta}}}{J_y} \dot{\theta} \\ \frac{(J_x - J_y)}{J_z} \dot{\phi}\dot{\theta} - \frac{k_{r_{drag\psi}}}{J_z} \dot{\psi} \end{bmatrix} \\ \delta &= \left[\frac{d_{l_1}}{m_t}, \frac{d_{l_2}}{m_t}, \frac{d_{l_3}}{m_t}, \frac{d_{r_1}}{J_x}, \frac{d_{r_2}}{J_y}, \frac{d_{r_3}}{J_z} \right]^T \\ b &= \left[\frac{1}{m_t}, \frac{1}{m_t}, \frac{1}{m_t}, \frac{1}{J_x}, \frac{1}{J_y}, \frac{1}{J_z} \right]^T \end{aligned} \quad (19)$$

A. Sliding surface design

Let $e \in \mathbb{R}^6$ be the tracking error of the system which is given as:

$$e = \chi_d - \chi \quad (20)$$

where $\chi = [x, y, z, \phi, \theta, \psi]^T$ and $\chi_d = [x_d, y_d, z_d, \phi_d, \theta_d, \psi_d]^T$ are the actual and desired position and orientation of the entire

system, respectively. For the system in Equation (16) and the tracking error in Equation (20), the Non-singular Fast Terminal Sliding Mode (NFTSM) surfaces are considered as follows:

$$\begin{cases} S_x &= \dot{e}_x + \xi e_x + \eta \text{sgn}(e_x)^a \\ S_y &= \dot{e}_y + \xi e_y + \eta \text{sgn}(e_y)^a \\ S_z &= \dot{e}_z + \xi e_z + \eta \text{sgn}(e_z)^a \\ S_\phi &= \dot{e}_\phi + \xi e_\phi + \eta \text{sgn}(e_\phi)^a \\ S_\theta &= \dot{e}_\theta + \xi e_\theta + \eta \text{sgn}(e_\theta)^a \\ S_\psi &= \dot{e}_\psi + \xi e_\psi + \eta \text{sgn}(e_\psi)^a \end{cases} \quad (21)$$

where $\xi > 0$, $\eta > 0$, $a \geq 1$, $\text{sgn}(e)^a = |e|^a \text{sgn}(e)$ and its derivative is given as [47] $\frac{d}{dt}(\text{sgn}(e)^a) = a|e|^{a-1}\dot{e}$, and $\text{sgn}(\cdot)$ is the sign function which is given in Equation (22):

$$\text{sgn}(e) := \begin{cases} 1 & \text{if } e > 0, \\ 0 & \text{if } e = 0, \\ -1 & \text{if } e < 0 \end{cases} \quad (22)$$

For simplicity of analysis and calculation, let $S = [S_x, S_y, S_z, S_\phi, S_\theta, S_\psi]^T$ represent the general NFTSM surface of all system variables above, and it is given as follows:

$$S = \dot{e} + \xi e + \eta |e|^a \text{sgn}(e) \quad (23)$$

Taking the time derivative of the sliding surface in Equation (23) results in:

$$\begin{aligned} \dot{S} &= \ddot{e} + \xi \dot{e} + \eta a |e|^{a-1} \dot{e} \\ &= \ddot{\chi}_d - \ddot{\chi} + \xi \dot{e} + \eta a |e|^{a-1} \dot{e} \end{aligned} \quad (24)$$

Substituting Equation (16) into Equation (24) results in:

$$\dot{S} = \ddot{\chi}_d - F - \delta - bu + (\xi + \eta a |e|^{a-1}) \dot{e} \quad (25)$$

Considering \hat{u} as an equivalent controller (continuous control law) to achieve $\dot{S} = 0$, results in the following:

$$\hat{u} = \frac{1}{b} [\ddot{\chi}_d - F - \delta + (\xi + \eta a |e|^{a-1}) \dot{e}] \quad (26)$$

To address dynamic uncertainties and external disturbances, as well as to increase the speed of convergence to the sliding surface, the control law can be formulated by incorporating a discontinuous term into \hat{u} in Equation (26) as follows:

$$u = \hat{u} + \frac{1}{b} [\lambda_1 S + \lambda_2 \text{sgn}(S)] \quad (27)$$

where $\lambda_1 > 0$ and $\lambda_2 > 0$.

B. Stability Analysis

Theorem 1. Consider the system dynamics in (16) and the proposed NFTSMC surfaces described in Equation (23). The proposed controller designed presented in Equation (27) ensures asymptotic stability of the closed loop system in the sense of Lyapunov.

Proof: to prove the stability of the system using the Lyapunov method. Let V be a Lyapunov function candidate for the system as follows:

$$V = \frac{1}{2} S^2 \quad (28)$$

where $V = 0$ when $S = 0$, and $V > 0$, $\forall S \neq 0$, and its time derivative exists and given as follows:

$$\dot{V} = S \dot{S} \quad (29)$$

Substituting Equation (25) into Equation (29) results in the following:

$$\dot{V} = [\ddot{\chi}_d - F - \delta - bu + (\xi + \eta a |e|^{a-1}) \dot{e}] S \quad (30)$$

Substituting Equation (27) into Equation (30) results in the following:

$$\begin{aligned} \dot{V} &= [-\lambda_1 S - \lambda_2 \text{sgn}(S)] S \\ &= -\lambda_1 S^2 - \lambda_2 |S| \end{aligned} \quad (31)$$

Since $\lambda_1 > 0 \implies \lambda_1 S^2 > 0$, $\forall S \neq 0$, Also, $\lambda_2 > 0 \implies \lambda_2 |S| > 0$, $\forall S \neq 0$. Therefore, $\dot{V} < 0$, $\forall S \neq 0 \implies \dot{V} \leq 0$, $\forall S$ which satisfies the Lyapunov stability condition and implies that the states will converge to the NFTSM surfaces ($S = 0$) as well as the errors will asymptotically converge to the origin.

Lemma 1. Using proposed controller in Equation (27), the system trajectories can reach the equilibrium state on the NFTSM sliding surface ($S = 0$) within a finite time.

Proof: to prove that the states of the system converge to the NFTSM surfaces ($S = 0$) in a finite time, lets use the result of Theorem 1 in Equation (31) to derive the reaching time (t_r) as follows:

$$\dot{V} = \frac{dV}{dt} = -\lambda_1 S^2 - \lambda_2 |S| \quad (32)$$

Using Equation (28), Equation (32) can be rewritten as follows:

$$\frac{dV}{dt} \leq -2\lambda_1 V - \lambda_2 \sqrt{2V}, \quad \text{such that:}$$

$$dt \leq \frac{-dV}{2\lambda_1 V + \gamma V^{\frac{1}{2}}} \quad (33)$$

Where $\gamma = \sqrt{2}\lambda_2$, then integrate both sides of Equation (33) such that:

$$\int_0^{t_r} dt \leq \int_{V(0)}^{V(t_r)} \frac{-dV}{2\lambda_1 V + \gamma V^{\frac{1}{2}}} \quad (34)$$

Using substitution to integrate the right side of Equation (34), we obtain:

$$\begin{aligned} \int_{V(0)}^{V(t_r)} \frac{-dV}{2\lambda_1 V + \gamma V^{\frac{1}{2}}} &= -\frac{1}{\lambda_1} \left[\ln |2\lambda_1 V^{\frac{1}{2}} + \gamma| \right]_{V(0)}^{V(t_r)} \\ &= \frac{1}{\lambda_1} \ln \left| \frac{2\lambda_1 V(0)^{\frac{1}{2}} + \gamma}{2\lambda_1 V(t_r)^{\frac{1}{2}} + \gamma} \right| \end{aligned} \quad (35)$$

Integrating the left side of Equation (34) and using the result in Equation (35), the reaching time (t_r) is given as:

$$t_r \leq \frac{1}{\lambda_1} \ln \left| \frac{2\lambda_1 V(0)^{\frac{1}{2}} + \gamma}{\gamma} \right| \quad (36)$$

Based on (36), Lemma 1 is proven and the system trajectories will reach ($S = 0$) within a finite time.

C. Position Controller

Using the controller designed in Equation (27), the virtual control inputs can be expressed as follows:

$$\begin{cases} u_x = m_t \ddot{x}_d + k_{l_{drag_x}} \dot{x} - d_{l_1} \\ \quad + m_t ((\xi + \eta a |e_x|^{a-1}) \dot{e}_x + \lambda_1 S_x + \lambda_2 \text{sgn}(S_x)) \\ u_y = \ddot{y}_d + k_{l_{drag_y}} \dot{y} - d_{l_2} \\ \quad + m_t ((\xi + \eta a |e_y|^{a-1}) \dot{e}_y + \lambda_1 S_y + \lambda_2 \text{sgn}(S_y)) \\ u_z = m_t \ddot{z}_d + m_t g + k_{l_{drag_z}} \dot{z} - d_{l_3} \\ \quad + (\xi + \eta a |e_z|^{a-1}) \dot{e}_z + \lambda_1 S_z + \lambda_2 \text{sgn}(S_z) \end{cases} \quad (37)$$

According to Equations (18) and (37), the total thrust U_1 is given as follows:

$$\begin{aligned} U_1 = & \frac{m_t}{c\phi c\theta} \left(\ddot{z}_d + g + \frac{1}{m_t} k_{l_{drag_z}} \dot{z} - \frac{d_{l_3}}{m_t} \right) \\ & + \frac{m_t}{c\phi c\theta} ((\xi + \eta a |e_z|^{a-1}) \dot{e}_z + \lambda_1 S_z + \lambda_2 \text{sgn}(S_z)) \end{aligned} \quad (38)$$

and the desired roll and pitch angles (ϕ_d and θ_d) can be calculated by utilizing the tangent function within limits $(-\frac{\pi}{2}, \frac{\pi}{2})$ of Euler angles, as follows:

$$\begin{aligned} \theta_d &= \arctan \left(\frac{u_x \cos(\psi_d) + u_y \sin(\psi_d)}{u_z} \right), \\ \phi_d &= \arctan \left(\cos(\theta_d) \left(\frac{u_x \sin(\psi_d) - u_y \cos(\psi_d)}{u_z} \right) \right) \end{aligned} \quad (39)$$

D. Attitude Controller

The attitude controller takes the desired roll and pitch angles (ϕ_d and θ_d) that are generated by the position controller in Equation (39) with the desired yaw angle ψ_d which is set by the designer according to the configuration of entire system to calculate the rolling, pitching, and yawing moments according to the general controller law in Equation (27) as follows:

$$\begin{aligned} U_2 &= J_x \left(\ddot{\phi}_d - \frac{(J_y - J_z)}{J_x} \dot{\theta} \dot{\psi} + \frac{k_{r_{drag_\phi}}}{J_x} \dot{\phi} - \frac{d_{r_1}}{J_x} \right) \\ &+ J_x ((\xi + \eta a |e_\phi|^{a-1}) \dot{e}_\phi + \lambda_1 S_\phi + \lambda_2 \text{sgn}(S_\phi)) \\ U_3 &= J_y \left(\ddot{\theta}_d - \frac{(J_z - J_x)}{J_y} \dot{\phi} \dot{\psi} + \frac{k_{r_{drag_\theta}}}{J_y} \dot{\theta} - \frac{d_{r_2}}{J_y} \right) \\ &+ J_y ((\xi + \eta a |e_\theta|^{a-1}) \dot{e}_\theta + \lambda_1 S_\theta + \lambda_2 \text{sgn}(S_\theta)) \\ U_4 &= J_z \left(\ddot{\psi}_d - \frac{(J_x - J_y)}{J_z} \dot{\phi} \dot{\theta} + \frac{k_{r_{drag_\psi}}}{J_z} \dot{\psi} - \frac{d_{r_3}}{J_z} \right) \\ &+ J_z ((\xi + \eta a |e_\psi|^{a-1}) \dot{e}_\psi + \lambda_1 S_\psi + \lambda_2 \text{sgn}(S_\psi)) \end{aligned} \quad (40)$$

E. Chattering Problem

Chattering occurs due to the discontinuous nature of the control law in sliding mode control (SMC). The control signal rapidly switches between two values, causing high-frequency oscillations around the sliding surface. Chattering can lead to mechanical wear, instability, and poor performance of actuators. Using sign function causes the chattering problem in

the control signal which is undesirable for the aforementioned reasons and needs to be eliminated. To achieve this, the control discontinuity can be smoothed out in a thin boundary layer in vicinity of the switching surface by using hyperbolic tangent function \tanh or saturation function sat which is given in Equation (41) as follows:

$$\text{sat}(S) := \begin{cases} 1 & \text{if } S > \Phi, \\ \frac{S}{\Phi} & \text{if } |S| \leq \Phi, \\ -1 & \text{if } S < -\Phi \end{cases} \quad (41)$$

where $0 < \Phi < 1$ represents the thin boundary layer. Modifying the controllers in Equations (38) and (40), the chattering-free controllers are given as follows:

$$\begin{aligned} U_1 &= \frac{m_t}{c\phi c\theta} \left(\ddot{z}_d + g + \frac{1}{m_t} k_{l_{drag_z}} \dot{z} - \frac{d_{l_3}}{m_t} \right) \\ &+ \frac{m_t}{c\phi c\theta} ((\xi + \eta a |e_z|^{a-1}) \dot{e}_z + \lambda_1 S_z + \lambda_2 \text{sat}(S_z/\Phi)) \\ U_2 &= J_x \left(\ddot{\phi}_d - \frac{(J_y - J_z)}{J_x} \dot{\theta} \dot{\psi} + \frac{k_{r_{drag_\phi}}}{J_x} \dot{\phi} - \frac{d_{r_1}}{J_x} \right) \\ &+ J_x ((\xi + \eta a |e_\phi|^{a-1}) \dot{e}_\phi + \lambda_1 S_\phi + \lambda_2 \text{sat}(S_\phi/\Phi)) \\ U_3 &= J_y \left(\ddot{\theta}_d - \frac{(J_z - J_x)}{J_y} \dot{\phi} \dot{\psi} + \frac{k_{r_{drag_\theta}}}{J_y} \dot{\theta} - \frac{d_{r_2}}{J_y} \right) \\ &+ J_y ((\xi + \eta a |e_\theta|^{a-1}) \dot{e}_\theta + \lambda_1 S_\theta + \lambda_2 \text{sat}(S_\theta/\Phi)) \\ U_4 &= J_z \left(\ddot{\psi}_d - \frac{(J_x - J_y)}{J_z} \dot{\phi} \dot{\theta} + \frac{k_{r_{drag_\psi}}}{J_z} \dot{\psi} - \frac{d_{r_3}}{J_z} \right) \\ &+ J_z ((\xi + \eta a |e_\psi|^{a-1}) \dot{e}_\psi + \lambda_1 S_\psi + \lambda_2 \text{sat}(S_\psi/\Phi)) \end{aligned} \quad (42)$$

F. Admittance Controller

Admittance controller is widely utilized in robotics and control systems [34], [44], [48], enabling a robot or a system to respond effectively to external forces or disturbances. It provides the robot with a degree of ‘‘softness’’ or ‘‘compliance’’, facilitating interaction with human and its environment in a safe and adaptive manner. In essence, the term ‘‘admittance’’ originates from electrical engineering, describing how a circuit reacts to an input voltage. In the realm of robotics, it has been adapted to characterize how a system reacts to external forces. The admittance controller enables attaining the desired interaction dynamics by adjusting the robot’s movement based on the measured or estimated interaction force. This control method governs the dynamic interaction between the motion parameters (such as position, velocity, and acceleration) and the input force by modifying the virtual inertia, damping, and stiffness of the robot. It simulates the behavior of the mass-damper-spring system through the mathematical relationship defined in Equation (43). Figure 3 depicts the behavior of the system as a mass-damper-spring system.

$$\mathbb{M}(\ddot{\mathbb{T}}_d - \ddot{\mathbb{T}}_r) + \mathbb{C}(\dot{\mathbb{T}}_d - \dot{\mathbb{T}}_r) + \mathbb{K}(\mathbb{T}_d - \mathbb{T}_r) = F_{ext} \quad (43)$$

where: $\mathbb{T}_d \in \mathbb{R}^3$ is the desired trajectory, $\mathbb{T}_r \in \mathbb{R}^3$ is the reference trajectory generated by the admittance controller according to human guidance proportional to the applied forces, $\mathbb{M} \in \mathbb{R}^{3 \times 3}$, $\mathbb{C} \in \mathbb{R}^{3 \times 3}$, $\mathbb{K} \in \mathbb{R}^{3 \times 3}$ are the diagonal

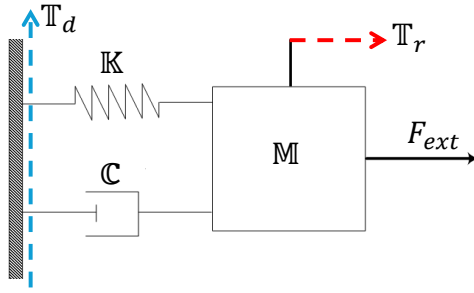


Fig. 3: Virtual mass-damper-spring system.

matrices of the virtual mass, damping, stiffness of the system, and $F_{ext} \in \mathbb{R}^3$ is the vector of external forces acting on the system due to human physical interaction and guidance. All quantities are expressed with respect to the inertial reference frame.

In this work, the admittance controller is designed to enable seamless interaction between human operator and aerial systems. It adjusts the aerial vehicle's behavior in real-time based on the force exerted by the human operator, allowing for precise control and coordination during payload transportation tasks. It generates a new reference trajectory proportional to the amount of the applied force as illustrated in Figure 4. The reference trajectories in Figure 4 represent the output of the admittance controller in response to the applied force in the (x, y, z) directions. The applied force is Gaussian-shaped, which is normalized in this graph.

The response of the physical interaction can be adapted by tuning the virtual spring stiffness constant \mathbb{K} . Increasing the value of \mathbb{K} produces a stiffer response while setting the value of \mathbb{K} to zero guarantees full compliance with the applied external force. The desired acceleration \ddot{T}_d and velocity \dot{T}_d are set to zero to enforce the system to maintain its position as long as no interaction force is applied. The controller architecture is optimized to ensure stability, robustness, and responsiveness in dynamic environments. In order to reject any environmental disturbances, the admittance controller response is triggered if the measured force exceeds a specific threshold.

IV. NUMERICAL RESULTS AND SIMULATION

A. Simulation Setup and Implementation

The simulation environment is configured to replicate real-world conditions and scenarios encountered during payload transportation tasks and physical interaction. In this section, we set up the simulation environment of the proposed assistive payload transportation system with human guidance thorough physical interaction. The system consists of two quadrotors and a common payload. The quadrotors are identical with known geometrical and physical specifications. The payload is a uniform beam-shaped circular bar. All components of

the system are rigidly connected, where each quadrotor is connected to each end of the payload. There are two force-torque sensors at the points of contact of rigid connection between the quadrotors and the payload to measure the interaction and reaction forces and torques between system's components as well as the human-robot physical interaction. The system operates near hovering state with small attitude angles. When the human operator applies force on the payload, the force will be measure by the force-torque sensors and send to the admittance controller. The latter regulates the virtual parameters of the system and generates a reference trajectory for the system to follow proportional to the amount and direction of the measured force according to human guidance. The reference trajectory is delivered to the position controller as a desired trajectory to generate the required thrust, as well as the desired orientation to the attitude controller to achieve the required movement and follow the human guidance with full compliance.

MATLAB is used as a simulation environment. The simulation is implemented to effectively assess the efficiency and performance of the control strategy suggested in Section III and stated in Equation (42). All simulation parameters, including individual quadrotor parameters, payload, the entire assistive payload transportation system, and the parameters of the position, attitude, and admittance controllers are given in Tables II and III, respectively. Additionally, the simulation environment is implemented using the Robotic Operation System (ROS noetic) and Gazebo 11, providing a realistic and flexible platform for experimentation. An IRIS quadrotor model was used to simulate the quadrotors and built the entire aerial vehicle. Figure 5.(a) shows the entire aerial vehicle built in Gazebo11 environment while Figure 5.(b) shows the MATLAB simulation of guided motion in 3D space of the assistive payload transportation system according to the human guidance and physical interaction. The human operator can apply forces on the payload in any direction to move the system to the direction of the applied force.

B. Numerical Results and Discussion

Extensive simulations were conducted to evaluate the performance of the proposed assistive payload transportation system with human physical interaction using quadrotors, as well as to assess the effectiveness of the proposed controller to stabilize the system and track the desired human guidance. The results indicate that the integration of human operators into the control loop of the system using the admittance controller significantly improves the payload transport capabilities. The system exhibits enhanced adaptability, flexibility, and safety, making it suitable for a wide range of applications in dynamic and unpredictable environments. At first, the aerial vehicle lifted the payload to a predefined height. At this moment, the admittance controller was engaged to be ready for physical interaction. As it is illustrated by red arrows in Figure 5.(b), a force was applied upward to place the aerial vehicle at an appropriate operating height. Then a simulated human guidance was performed by applying forces in different directions to transport the payload to the final destination. The results

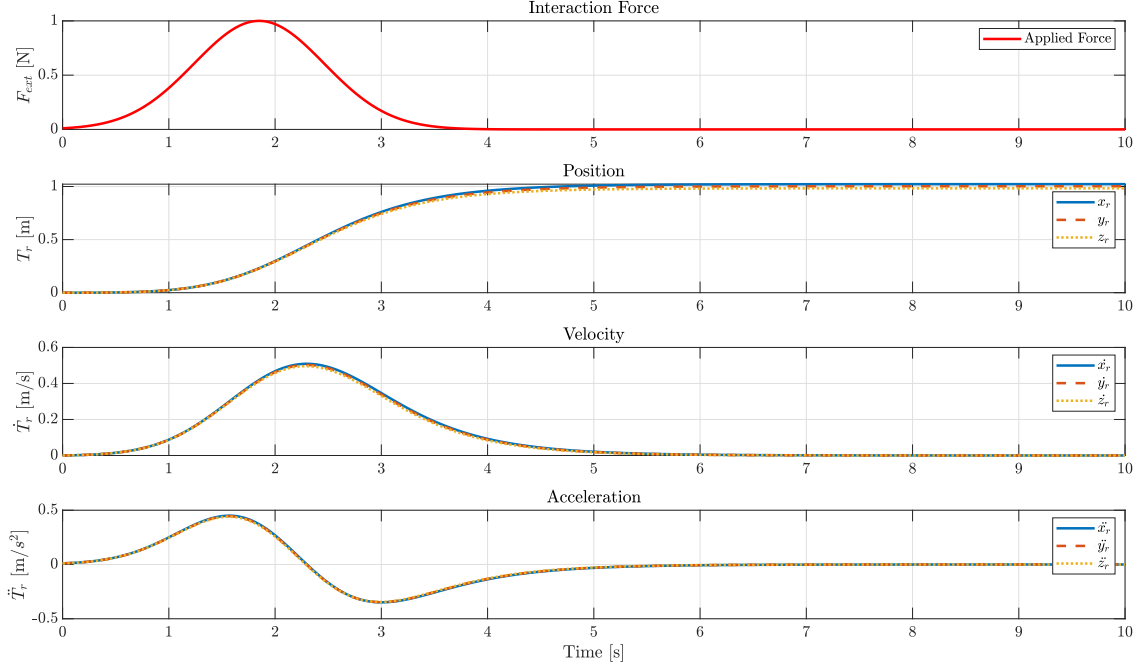


Fig. 4: Reference trajectories generated by the admittance controller proportional to the applied force.

TABLE II: System parameters.

Symbol	Definition	Value/ Unit
m_i	Mass of i^{th} quadrotor	1.5/kg
J_x	Moment of inertia of the x-axis	$2.9125 \times 10^{-2}/kg \ m^2$
J_y	Moment in inertia of the y-axis	$2.9125 \times 10^{-2}/kg \ m^2$
J_z	Moment in inertia of the z-axis	$5.5225 \times 10^{-2}/kg \ m^2$
l	Arm length of i^{th} quadrotor	0.25/m
m_L	Mass	0.5/kg
J_{Lx}	Moment of inertia of the x-axis	$16.6667 \times 10^{-2}/kg \ m^2$
J_{Ly}	Moment in inertia of the y-axis	$6.25 \times 10^{-4}/kg \ m^2$
J_{Lz}	Moment in inertia of the z-axis	$16.6667 \times 10^{-2}/kg \ m^2$
L	Length	2/m
r_L	Radius	0.05/m
m_t	Total mass of entire system	3.5/kg
g	Gravitational acceleration	9.81/m/s ²
J_{tx}	Moment of inertia of the x-axis	3.227327/kg m ²
J_{ty}	Moment of inertia of the y-axis	0.061286/kg m ²
J_{tz}	Moment of inertia of the z-axis	3.277117/kg m ²
$k_{l_{drag_x}}$	Drag coefficients along the x-axis	$6 \times 10^{-3}/N \ s/m$
$k_{l_{drag_y}}$	Drag coefficients along the y-axis	$6 \times 10^{-3}/N \ s/m$
$k_{l_{drag_z}}$	Drag coefficients along the z-axis	$6 \times 10^{-3}/N \ s/m$
$k_{r_{drag_\phi}}$	Drag coefficients about the x-axis	$6 \times 10^{-3}/N \ s$
$k_{r_{drag_\theta}}$	Drag coefficients about the y-axis	$6 \times 10^{-3}/N \ s$
$k_{r_{drag_\psi}}$	Drag coefficients about the z-axis	$6 \times 10^{-3}/N \ s$

TABLE III: Parameters of the Controller.

Symbol	Definition	Value/ Unit
ξ_x, ξ_y, ξ_z	Control constants	4, 2, 11
$\xi_\phi, \xi_\theta, \xi_\psi$	Control constants	25, 80, 25
η_x, η_y, η_z	Control constants	0.2, 0.1, 0.2
$\eta_\phi, \eta_\theta, \eta_\psi$	Control constants	0.2, 0.2, 0.2
$\lambda_{1x}, \lambda_{1y}, \lambda_{1z}$	Control constants	0.2, 0.1, 200
$\lambda_{2x}, \lambda_{2y}, \lambda_{2z}$	Control constants	2, 1, 100
$\lambda_{1\phi}, \lambda_{1\theta}, \lambda_{1\psi}$	Control constants	40, 40, 40
$\lambda_{2\phi}, \lambda_{2\theta}, \lambda_{2\psi}$	Control constants	30, 30, 30
a	Positive constant	3
\mathbb{M}	Virtual mass	1/kg
\mathbb{C}	Virtual damping coefficients	1.6/N s/m
\mathbb{K}	Virtual spring constants	0/N s/m

showed full compliance of the system with the applied human guidance, while the controller maintained the stability of the system during the process until the final destination. The results of the NFTSMC position and attitude controllers are illustrated as follows:

Figure 6 shows the performance results of the system and its trajectories including the desired and actual orientation, position, velocity, and tracking errors. The actual trajectories tracked the reference trajectories that were generated by the

admittance controller as desired trajectories for the position and attitude controllers. One can see that the controllers perfectly tracked the desired trajectories and followed the human operator's guidance. Additionally, the results show that the controllers were able to stabilize the system and reduced the errors to zero after an aggressive start at the beginning of the simulation. The first column of the figure shows the desired and actual orientation of the system (ϕ, θ, ψ) . It can be clearly seen that the position controller received the reference trajectories from the admittance controller and managed to generate the required thrust and desired orientation (ϕ_d) and (θ_d) . The desired orientation were delivered to the attitude controller while the latter tracked them to move the system to the positions in the x and y directions according to human guidance. Notice that the (ψ) angle is kept at zero as it desired by the designer. The second column shows the corresponding trajectories of the system in the (x, y, z) directions. The x graph shows the forward direction of the system which

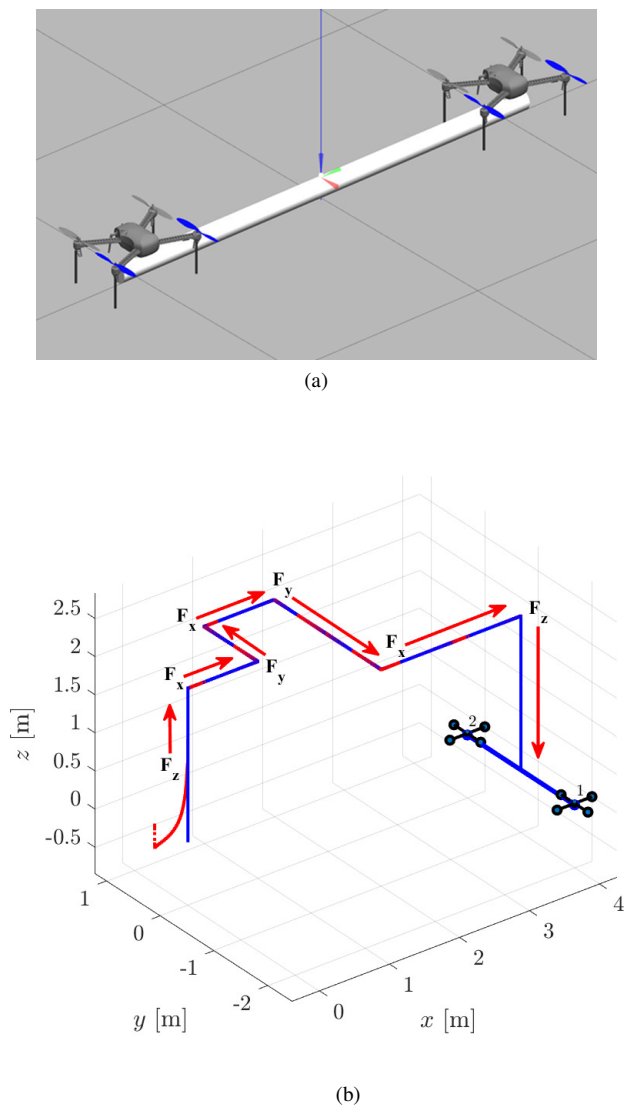


Fig. 5: The simulation environment setup; (a) The entire aerial vehicle built in ROS and Gazebo environment, (b) MATLAB simulation of the assistive system's motion following human guidance in 3D space as depicted by the red arrows.

gradually increased following the applied forces alongside with the velocity profile which went up and down for each movement, depicting the required increase in the velocity at the beginning of the movement and the decrease in the velocity as the system prepares for full stop waiting for upcoming physical interaction. In addition, the (y) direction graph shows that the system went left and right, navigating according to human guidance and the applied physical interaction force.

Moreover, the (z) direction graph shows that the altitude of the system increased to the appropriate operating height and maintained the same altitude until it reached the destination and finally landed while the velocity graph shows the related velocity profile. Furthermore, Figure 6 shows the normalized tracking errors of the system for the the orientation, position, and linear velocity, respectively. It can be noticed the errors of position and the velocity were driven to zero and kept at zero during the entire mission time, indicating the robust

performance of the proposed controller. On the other hand, the orientation error shows some fluctuations which are related to the high rolling and pitching control inputs at the start and stop points of the system due to high inertia, however the error is bounded and driven to zero by the controller at each point.

Figure 7 shows the calculated control inputs that include the total thrust, rolling, pitching, and yawing moments calculated according to the proposed NFTSMC position and attitude controllers. It can be seen that the controllers took appropriate actions to stabilize the system at the disturbed starting point in the beginning of the simulation. Then, they returned back to their normal rhythm to generate the control signals making the system performed appropriate navigation under the simulated human guidance. The human guidance and interaction with the system in a 3D environment is depicted in Figure 8. The plots illustrate the external forces applied (solid blue) on the center of mass (CoM) of the payload, alongside with the system's reference trajectories (dotted red) in the x , y , and z directions. The dashed black lines represent the thresholds that regulate the transition between the actions of the admittance controller (gray-shaded areas) and the position controller (white areas) which work together to achieve the transportation task.

Finally, Figure 9 shows the results of simulating the system using ROS and Gazebo environments. Figure 9.(a) shows the system at the starting position landing on the ground at the beginning of a zigzag corridor. Then, Figure 9.(b) shows the system navigating through the zigzag corridor according to the magnitudes and directions of the applies forces. Then Figure 9.(c) shows the system reaching the end of the zigzag corridor. Finally, Figure 9.(d) shows the system landing on the ground at the destination point at the end of a zigzag corridor. The human guidance was simulated by applying forces in any direction through the Gazebo interface.

V. CONCLUSION

In conclusion, this paper presents an assistive payload transportation using a dual-quadrotor UAVs system with physical human interaction. A novel Admittance-NFTSMC controller is utilized to control and stabilize the system to track human guidance. The stability of the proposed controller is proved using Lyapunov analysis. The proposed control strategy was validated through different numerical simulations conducted in MATLAB, ROS, and the Gazebo environments. The proposed system demonstrates its ability to perform well in terms of stability, fast response, and error convergence, highlighting its potential for practical implementation in industrial applications with unstructured environments. Future research directions include further optimization of the admittance controller, integration of advanced sensing and perception capabilities, and real-world experimentation to validate the effectiveness of the proposed approach.

VI. DISCLOSURE STATEMENT

No potential conflict of interest was reported by the author(s).

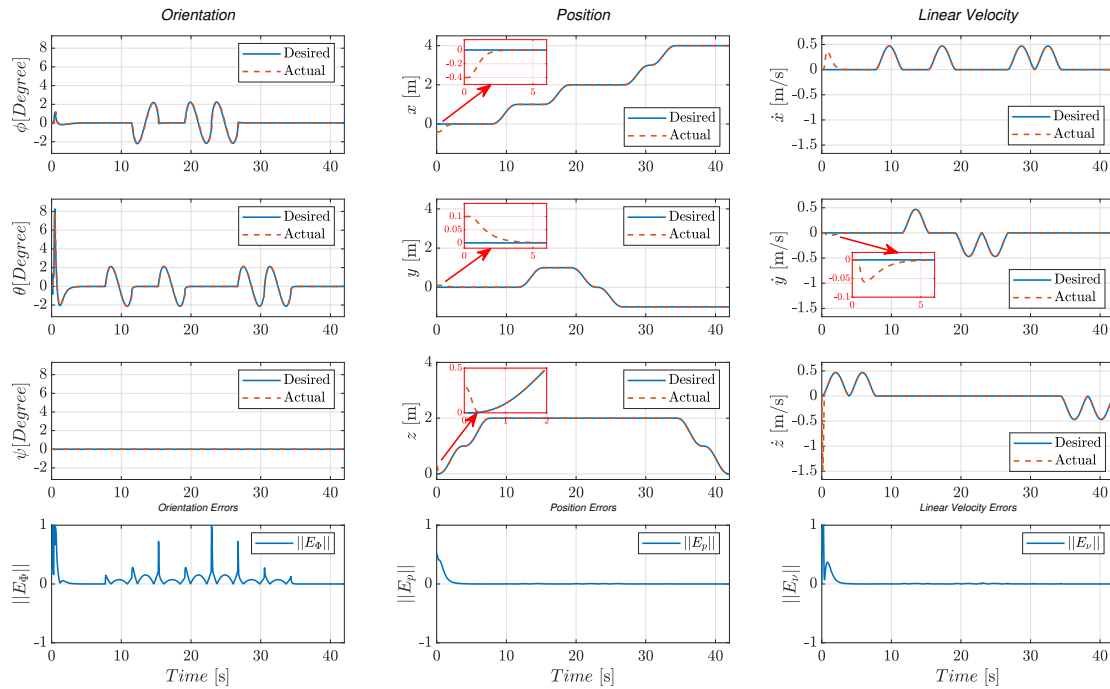


Fig. 6: The simulation results; First column for the desired and actual orientation of the system, Second column for the desired and actual positioning, Third column for the linear velocity of the system in (x, y, z) directions, and the bottom row for the normalized tracking errors of the system (orientation, position, and linear velocity).

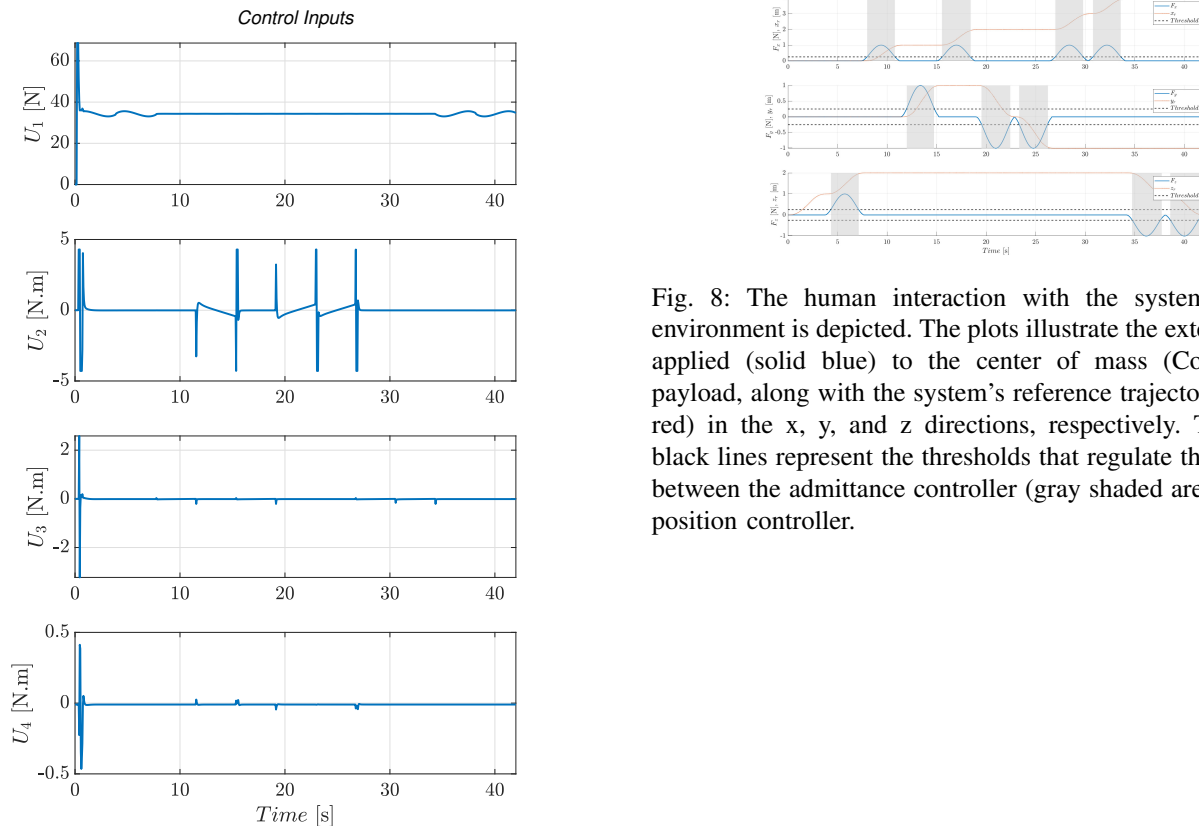


Fig. 7: The control inputs.

Fig. 8: The human interaction with the system in a 3D environment is depicted. The plots illustrate the external forces applied (solid blue) to the center of mass (CoM) of the payload, along with the system's reference trajectories (dotted red) in the x , y , and z directions, respectively. The dashed black lines represent the thresholds that regulate the transition between the admittance controller (gray shaded areas) and the position controller.

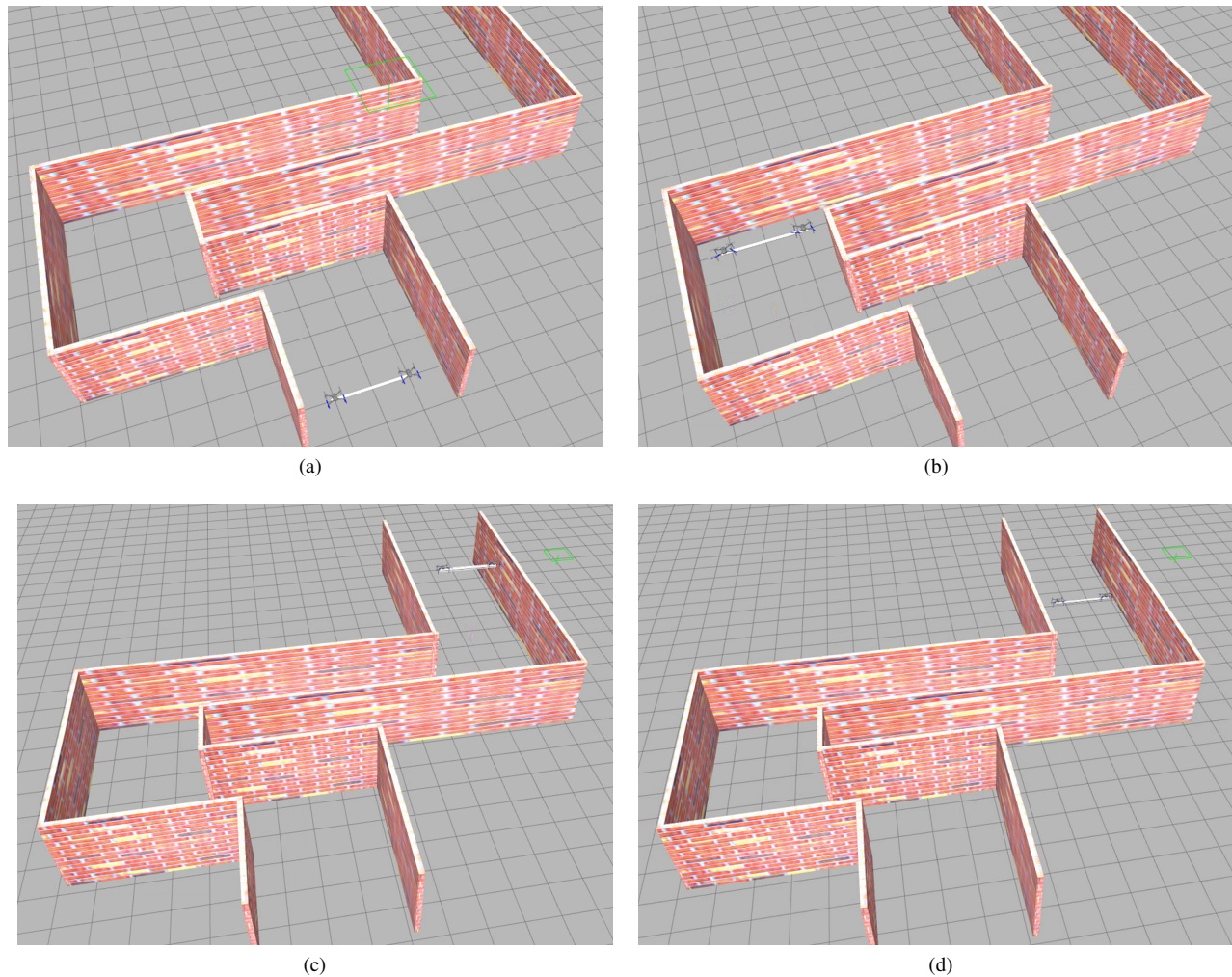


Fig. 9: The results of simulating the system in ROS and Gazebo environment; (a) The starting position at the beginning of a zigzag corridor, (b) The system navigating through the zigzag corridor, (c) The system reaching the end of the zigzag corridor, (d) The system landing on the ground in the destination point at the end of a zigzag corridor.

VII. DATA AVAILABILITY STATEMENT

The authors confirm that the data supporting the findings of this study are available with the supplementary materials of the article. The codes are available from the corresponding author upon reasonable request.

VIII. ACKNOWLEDGMENT

This work was supported in part by the National Sciences and Engineering Research Council of Canada (NSERC) under the grants RGPIN-2022-04937. The authors also acknowledge the support of the University of Thi-Qar, Iraqi Ministry of Higher Education and Scientific Research under financial support (No. 6608 in 21/06/2022).

REFERENCES

- [1] S. Khalid, F. Alnajjar, M. Gochoo, A. Renawi, and S. Shimoda, "Robotic assistive and rehabilitation devices leading to motor recovery in upper limb: a systematic review," *Disability and Rehabilitation: Assistive Technology*, vol. 18, no. 5, pp. 658–672, 2023.
- [2] H. Hasan, "A cost effective deaf-mute electronic assistant system using myo armband and smartphone," *International Journal of Science and Research (IJSR)*, vol. 6, pp. 950–954, 2017.
- [3] H. Naser, H. Hammood, and A. Q. Migot, "Internet-based smartphone system for after-stroke hand rehabilitation," in *2023 International Conference on Engineering, Science and Advanced Technology (ICESAT)*. IEEE, 2023, pp. 69–74.
- [4] R. Fuentes-Alvarez, J. H. Hernandez, I. Matehuala-Moran, M. Alfaro-Ponce, R. Lopez-Gutierrez, S. Salazar, and R. Lozano, "Assistive robotic exoskeleton using recurrent neural networks for decision taking for the robust trajectory tracking," *Expert Systems with Applications*, vol. 193, p. 116482, 2022.
- [5] H. N. Hasan, "A wearable rehabilitation system to assist partially hand paralyzed patients in repetitive exercises*," *Journal of Physics: Conference Series*, vol. 1279, no. 1, p. 012040, jul 2019.
- [6] J. Li and M. Ensafjoo, "It's not uav, it's me: Demographic and self-other effects in public acceptance of a socially assistive aerial manipulation system for fatigue management," *International Journal of Social Robotics*, vol. 16, no. 1, pp. 227–243, 2024.
- [7] M. Alkaddour, M. A. Jaradat, S. Tellab, N. Sherif, M. Alvi, L. Romdhane, and K. S. Hatamleh, "Novel design of lightweight aerial manipulator for solar panel cleaning applications," *IEEE Access*, 2023.
- [8] Z. Ghelichi, M. Gentili, and P. B. Mirchandani, "Drone logistics for uncertain demand of disaster-impacted populations," *Transportation research part C: emerging technologies*, vol. 141, p. 103735, 2022.
- [9] D. A. Rodríguez, C. L. Tafur, P. F. M. Daza, J. A. V. Vidales, and J. C. D. Rincón, "Inspection of aircrafts and airports using uas: a review," *Results in Engineering*, p. 102330, 2024.

- [10] P. Radoglou-Grammatikis, P. Sarigiannidis, T. Lagkas, and I. Moschios, "A compilation of uav applications for precision agriculture," *Computer Networks*, vol. 172, p. 107148, 2020.
- [11] S. Meesaragandla, M. P. Jagtap, N. Khatri, H. Madan, and A. A. Vadduri, "Herbicide spraying and weed identification using drone technology in modern farms: A comprehensive review," *Results in Engineering*, p. 101870, 2024.
- [12] G. Albeaino, M. Gheisari, and R. R. Issa, "Human-drone interaction (hdi): Opportunities and considerations in construction," *Automation and robotics in the architecture, engineering, and construction industry*, pp. 111–142, 2022.
- [13] J. M. Nwaogu, Y. Yang, A. P. Chan, and H.-I. Chi, "Application of drones in the architecture, engineering, and construction (aec) industry," *Automation in Construction*, vol. 150, p. 104827, 2023.
- [14] H. Ranjbar, P. Forsythe, A. A. F. Fini, M. Maghrebi, and T. S. Waller, "Addressing practical challenge of using autopilot drone for asphalt surface monitoring: Road detection, segmentation, and following," *Results in Engineering*, vol. 18, p. 101130, 2023.
- [15] M. A. Cheema, R. I. Ansari, N. Ashraf, S. A. Hassan, H. K. Qureshi, A. K. Bashir, and C. Politis, "Blockchain-based secure delivery of medical supplies using drones," *Computer Networks*, vol. 204, p. 108706, 2022.
- [16] I. H. B. Pizetta, A. S. Brandão, and M. Sarcinelli-Filho, "Load transportation by quadrotors in crowded workspaces," *IEEE Access*, vol. 8, pp. 223 941–223 951, 2020.
- [17] Z. Ghelichi, M. Gentili, and P. B. Mirchandani, "Logistics for a fleet of drones for medical item delivery: A case study for louisville, ky," *Computers & Operations Research*, vol. 135, p. 105443, 2021.
- [18] H. A. Hashim, "Exponentially stable observer-based controller for VTOL-UAVs without velocity measurements," *International Journal of Control*, vol. 96, no. 8, pp. 1946–1960, 2023.
- [19] D. K. Villa, A. S. Brandao, and M. Sarcinelli-Filho, "A survey on load transportation using multirotor uavs," *Journal of Intelligent & Robotic Systems*, vol. 98, pp. 267–296, 2020.
- [20] H. A. Hashim, A. E. Eltoukhy, and A. Odry, "Observer-based controller for VTOL-UAVs tracking using direct vision-aided inertial navigation measurements," *ISA transactions*, vol. 137, pp. 133–143, 2023.
- [21] H. Xie, K. Dong, and P. Chirarattananon, "Cooperative transport of a suspended payload via two aerial robots with inertial sensing," *IEEE Access*, vol. 10, pp. 81 764–81 776, 2022.
- [22] P.-X. Wu, C.-C. Yang, and T.-H. Cheng, "Cooperative transportation of uavs without inter-uav communication," *IEEE/ASME Transactions on Mechatronics*, 2023.
- [23] X. Liang, Z. Su, W. Zhou, G. Meng, and L. Zhu, "Fault-tolerant control for the multi-quadrotors cooperative transportation under suspension failures," *Aerospace Science and Technology*, vol. 119, p. 107139, 2021.
- [24] A. Shevidi and H. A. Hashim, "Quaternion-based adaptive backstepping fast terminal sliding mode control for quadrotor UAVs with finite time convergence," *Results in Engineering*, p. 102497, 2024.
- [25] Y. Liu, F. Zhang, P. Huang, and X. Zhang, "Analysis, planning and control for cooperative transportation of tethered multi-rotor uavs," *Aerospace Science and Technology*, vol. 113, p. 106673, 2021.
- [26] B. Shirani, M. Najafi, and I. Izadi, "Cooperative load transportation using multiple uavs," *Aerospace Science and Technology*, vol. 84, pp. 158–169, 2019.
- [27] S. Barawkar, M. Kumar, and M. Bolender, "Decentralized adaptive controller for multi-drone cooperative transport with offset and moving center of gravity," *Aerospace Science and Technology*, vol. 145, p. 108960, 2024.
- [28] J. Cai and B. Xian, "Robust hierarchical geometry control for the multiple uavs aerial transportation system with a suspended payload," *Nonlinear Dynamics*, pp. 1–21, 2024.
- [29] H. A. Hashim, A. E. Eltoukhy, and K. G. Vamvoudakis, "UWB ranging and IMU data fusion: Overview and nonlinear stochastic filter for inertial navigation," *IEEE Transactions on Intelligent Transportation Systems*, 2023.
- [30] J. Espin, C. Camacho, and O. Camacho, "Control of non-self-regulating processes with long time delays using hybrid sliding mode control approaches," *Results in Engineering*, vol. 22, p. 102113, 2024.
- [31] R. Alike, E. M. Mellouli, and E. H. Tissir, "A modified sliding mode controller based on fuzzy logic to control the longitudinal dynamics of the autonomous vehicle," *Results in Engineering*, p. 102120, 2024.
- [32] L. Medina, G. Guerra, M. Herrera, L. Guevara, and O. Camacho, "Trajectory tracking for non-holonomic mobile robots: A comparison of sliding mode control approaches," *Results in Engineering*, p. 102105, 2024.
- [33] M. said Adouairi, B. Bossoufi, S. Motahhir, and I. Saady, "Application of fuzzy sliding mode control on a single-stage grid-connected pv system based on the voltage-oriented control strategy," *Results in Engineering*, vol. 17, p. 100822, 2023.
- [34] A. Tagliabue, M. Kamel, S. Verling, R. Siegwart, and J. Nieto, "Collaborative transportation using mavs via passive force control," in *2017 IEEE International Conference on Robotics and Automation (ICRA)*, 2017, pp. 5766–5773.
- [35] J. Horyna, T. Baca, and M. Saska, "Autonomous collaborative transport of a beam-type payload by a pair of multi-rotor helicopters," in *2021 International Conference on Unmanned Aircraft Systems (ICUAS)*, 2021, pp. 1139–1147.
- [36] G. Loianno and V. Kumar, "Cooperative transportation using small quadrotors using monocular vision and inertial sensing," *IEEE Robotics and Automation Letters*, vol. 3, no. 2, pp. 680–687, 2018.
- [37] H. A. Hashim and F. L. Lewis, "Nonlinear stochastic estimators on the special euclidean group SE (3) using uncertain imu and vision measurements," *IEEE Transactions on Systems, Man, and Cybernetics: Systems*, vol. 51, no. 12, pp. 7587–7600, 2022.
- [38] H. A. Hashim, "Systematic convergence of nonlinear stochastic estimators on the special orthogonal group SO (3)," *International Journal of Robust and Nonlinear Control*, vol. 30, no. 10, pp. 3848–3870, 2020.
- [39] A. Rajaeizadeh, A. Naghash, and A. Mohamadifard, "Cooperative aerial payload transportation using two quadrotors," in *Proceedings of the International micro air vehicle conference and flight competition*, 2017, pp. 73–80.
- [40] D. Mellinger, M. Shomin, N. Michael, and V. Kumar, "Cooperative grasping and transport using multiple quadrotors," in *Distributed Autonomous Robotic Systems: The 10th International Symposium*. Springer, 2013, pp. 545–558.
- [41] F. Augugliaro and R. D'Andrea, "Admittance control for physical human-quadrocopter interaction," in *2013 European Control Conference (ECC)*. IEEE, 2013, pp. 1805–1810.
- [42] P. Prajapati and V. Vashista, "Aerial physical human robot interaction for payload transportation," *IEEE Robotics and Automation Letters*, 2023.
- [43] M. Xu, A. Hu, and H. Wang, "Visual-impedance-based human-robot cotransportation with a tethered aerial vehicle," *IEEE Transactions on Industrial Informatics*, vol. 19, no. 10, pp. 10 356–10 365, 2023.
- [44] M. Romano, A. Ye, J. Pye, and E. Atkins, "Cooperative multilift slung load transportation using haptic admittance control guidance," *Journal of Guidance, Control, and Dynamics*, vol. 45, no. 10, pp. 1899–1912, 2022.
- [45] H. A. Hashim, "Special Orthogonal Group SO(3), Euler Angles, Angle-axis, Rodriguez Vector and Unit-quaternion: Overview, Mapping and Challenges," *arXiv preprint arXiv:1909.06669*, 2019.
- [46] H. A. Hashim, L. J. Brown, and K. McIsaac, "Nonlinear stochastic attitude filters on the special orthogonal group 3: Ito and Stratonovich," *IEEE Transactions on Systems, Man, and Cybernetics: Systems*, vol. 49, no. 9, pp. 1853–1865, 2019.
- [47] M. Boukattaya, N. Mezghani, and T. Damak, "Adaptive nonsingular fast terminal sliding-mode control for the tracking problem of uncertain dynamical systems," *ISA transactions*, vol. 77, pp. 1–19, 2018.
- [48] M. Tognon, R. Alami, and B. Siciliano, "Physical human-robot interaction with a tethered aerial vehicle: Application to a force-based human guiding problem," *IEEE Transactions on Robotics*, vol. 37, no. 3, pp. 723–734, 2021.